Applied Catalysis B: Environmental 134–135 (2013) 286–292

Contents lists available at SciVerse ScienceDirect

Applied Catalysis B: Environmental

journal homepage: www.elsevier.com/locate/apcatb

A new heterojunction Ag_3PO_4/Cr-$SrTiO_3$ photocatalyst towards efficient elimination of gaseous organic pollutants under visible light irradiation

Jianjun Guo [a,b,c], Shuxin Ouyang [b,**], Peng Li [a,b,c], Yuanjian Zhang [d], Tetsuya Kako [a,b,c], Jinhua Ye [a,b,c,e,*]

[a] Graduate School of Chemical Sciences and Engineering, Hokkaido University, Sapporo, Japan
[b] Environmental Remediation Materials Unit, National Institute for Materials Science (NIMS), 1-1 Namiki, Tsukuba, Ibaraki, Japan
[c] International Center for Materials Nanoarchitectonics (WPI-MANA), National Institute for Materials Science (NIMS), 1-1 Namiki, Tsukuba, Ibaraki, Japan
[d] International Center for Young Scientists (ICYS) & International Center for Materials Nanoarchitections (WPI-MANA), National Institute for Materials Science (NIMS), Japan
[e] TU-NIMS Joint Research Center, School of Materials Science and Engineering, Tianjin University, 92 Weijin Road, Nankai District, Tianjin, PR China

ARTICLE INFO

Article history:
Received 11 October 2012
Received in revised form
28 December 2012
Accepted 30 December 2012

Keywords:
Ag_3PO_4/Cr-$SrTiO_3$
Heterojunction
IPA photodegradation
Photocatalysis

ABSTRACT

A new heterojunction Ag_3PO_4/Cr-$SrTiO_3$ was designed to eliminate the gaseous pollutants under visible light irradiation. The phase compositions, optical properties, and morphologies of the heterojunction photocatalysts were systematically investigated via powder X-ray diffraction, UV–Visible absorption spectroscopy, scanning electron microscopy and energy-dispersive X-ray spectroscopy, and transmission electron microscopy. The photodegradation of Isopropyl alcohol (IPA) was carried out to test the photocatalytic activity of the heterojunction. The results revealed that the heterojunction exhibited considerably improved efficiency in IPA photodegradation (CO_2, 13.2 ppm h^{-1}) in comparison with pure Ag_3PO_4 (CO_2, 0.4 ppm h^{-1}) and Cr-$SrTiO_3$ (CO_2, 1.9 ppm h^{-1}) under visible light irradiation. In addition, the effects of mixing ratio and calcination temperature of the heterojunction were studied. The highest activity was observed in the Ag_3PO_4/Cr-$SrTiO_3$ heterojunction with the mass ratio of 1:4 (Ag_3PO_4:Cr-$SrTiO_3$) sintered at 500 °C. An investigation of energy-band structure via valence-band X-ray photoelectron spectrum indicates that the conduction band (CB) and valence band (VB) of Ag_3PO_4 are both more positive than that of Cr-$SrTiO_3$, which facilitates the separation and transfer of photogenerated electrons and holes between the two photocatalysts.

1. Introduction

Semiconductor-based photocatalysts have attracted worldwide attention, because they can eliminate environmental pollutants and produce clean H_2 energy by utilizing solar energy efficiently [1–5]. During the past decades, TiO_2 [6–8] has been widely investigated as a classic photocatalyst. However, its band gap is so wide that it can only absorb the UV light which occupies about 4% in solar light. Therefore, in recent years, much effort has been focused on searching for other efficient photocatalysts that are active under visible-light irradiation. On this theme, various semiconductors have been developed, such as modified-TiO_2 [9–13], multimental oxides [14–16], sulfides [17,18], oxynitrides [19–21] and heterojunctions [22–24].

Among these photocatalysts, silver orthophosphate (Ag_3PO_4) as a novel photocatalyst with promising efficiency in water oxidiation and photodecomposition of organic dyes was reported recently [25a]. More specifically, Ag_3PO_4 can achieve a quantum efficiency of about 90% at wavelength around 420 nm in water oxidation, which is significantly higher than that of other previously reported semiconductors. Moreover, further investigations about the photoelectric/photocatalytic properties, morphology controlling, and facet effect of Ag_3PO_4 were carried out, and enhanced performances were obtained [25b–e]. However, the efficiency of Ag_3PO_4 in photodecomposition of gaseous organic contaminants is still needed to improved. One reason is that its potential of the conduction band (CB) is more positive than the reduction potential of O_2 ($e^- + O_2 + H^+ \rightarrow HO_2$, −0.046 V vs. NHE) [26,27]. As a result, the generated electrons cannot be consumed by combining with O_2 which is very important for the photooxidization of the gaseous organic compound [5]. Another reason is that the decomposition of IPA to CO_2 is a complex multiphoton-involved process ($CH_3CHOHCH_3 + 5H_2O + 18\,h^+ \rightarrow 3CO_2 + 18H^+$) [44], which cannot easily be realized on pure Ag_3PO_4. Moreover, as the electrode potential of Ag_3PO_4/Ag (around 0.45 V vs. NHE) is more positive than that of H^+/H_2 (0 V vs. NHE) [27], Ag_3PO_4 can easily

* Corresponding author at: International Center for Materials Nanoarchitectonics (WPL-MANA), National Institute for Materials Science (NIMS), 1-1 Namiki, Tsukuba, Ibaraki, Japan.
** Corresponding author.
E-mail addresses: OUYANG.Shuxin@nims.go.jp (S. Ouyang), Jinhua.YE@nims.go.jp (J. Ye).

0926-3373/$ – see front matter © 2013 Elsevier B.V. All rights reserved.
http://dx.doi.org/10.1016/j.apcatb.2012.12.038

be reduced to Ag^0 during in the photocatalytic reactions. Constructing a heterojunction between Ag_3PO_4 and another semiconductor with proper band structure can induce multi-electron reaction ($2e^- + O_2 + 2H^+ \rightarrow H_2O_2$, 0.695 V vs. NHE), and can accumulate holes on the valence band of Cr-$SrTiO_3$ for the multiphoton-involved process, which will effectively solve the above-mentioned problems.

In previous studies, numerous heterostructured photocatalysts, such as TiO_2 [28,29], $SrTiO_3$ [30,31], and ZnO [32,33] coupled with different photocatalysts, have been designed and tested for photodegradation of the pollutants. However, there are few examples of heterostructured photocatalysts based on Ag_3PO_4 [25e,34]. Compared with above mentioned semiconductors, Cr-doped $SrTiO_3$ is a semiconductor photocatalyst with narrower band gap (about 1.9 eV), which can adsorb the visible light with wavelength as long as 600 nm and exhibit remarkable efficiency in H_2 evolution [35]. Furthermore, the band gap of Ag_3PO_4 is 2.45 eV, and its conduction band (CB) and valence band (VB) positions are +0.45 and +2.90 eV (vs. NHE), respectively [25a]. In view of the chemical potential, the CB and VB levels of Cr doped $SrTiO_3$ are appreciably more negative than that of Ag_3PO_4. Thus, Cr-doped $SrTiO_3$ and Ag_3PO_4 are two appropriate candidates to construct a heterostructured photocatalyst to work under visible-light irradiation. Hence, in this work, we synthesized a novel heterostructured photocatalyst based on Ag_3PO_4 and Cr doped $SrTiO_3$ via a solid calcination method. Isopropanol (IPA) photodegradation over the heterojunctions under visible-light irradiation was employed for evaluating their photocatalytic properties. The effects of different mass ratio and calcination temperature on photocatalytic activity were systematically investigated. In particular, the valence-band state of Ag_3PO_4 and Cr doped $SrTiO_3$ were analyzed by X-ray photoelectron spectroscopy (XPS) to deduce the band structures, which helps understand the transfer of photocarriers between the two semiconductors.

2. Experimental

2.1. Photocatalysts preparation

All of the reagents were analytical grade and used without further purification. The Cr doped $SrTiO_3$ (Cr-$SrTiO_3$) was synthesized similar to our previous reports [36]. In detail, stoichiometric titanium isopropylate ($[(CH_3)_2CHO]_4Ti$), strontium acetate ($Sr(Ac)_2{\cdot}0.5H_2O$), and $Cr(NO_3)_3{\cdot}9H_2O$ were mixed thoroughly in ethylene glycol (dehydrated) with a molar ratio of 1:0.95:0.05, respectively. The mixed solution was heated at 70 °C until the reagents totally volatilized to obtain a gel. After grinding the gel completely, the obtained powders were added into 80 mL of aqueous NaOH aqueous solution (5 mol L^{-1}), and then the mixture was poured into 120 ml of a Teflon-lined stainless steel autoclave. This autoclave was heated up to 180 °C and kept for 36 h. The obtained precipitate was washed several times with distilled water for several times and dried at room temperature overnight. The Ag_3PO_4 was synthesized by the ion-exchange method as described in our former report [25]. Appropriate amounts of $AgNO_3$ and Na_2HPO_4 were mixed and milled thoroughly until the initial color changed to yellow. The obtained precipitate was washed with distilled water for several times and dried at room temperature overnight. The Ag_3PO_4/Cr-$SrTiO_3$ heterojunctions with different mass ratios were prepared by grinding and mixing individual solids thoroughly in ethanol in an agate mortar. After that, the prepared samples were dried at 60 °C overnight and then calcined at different temperatures for 5 h in an oven, respectively.

2.2. Photocatalysts characterization

The physical property and photocatalytic activity of Ag_3PO_4 and Cr-$SrTiO_3$ were systematically investigated (details in supporting information, Fig. S1–S8). X-ray diffraction patterns were characterized with a Rigaku Rint-2000 X-ray diffractometer equipped with graphite monochromatized Cu Kα radiation (λ = 1.54178 Å). Scanning electron microscopy images and energy-dispersive X-ray spectroscopy patterns were recorded with a JEOL 6700F field emission scanning electron microscopy. Transmission electron microscope and high-resolution images were performed with a JEOL 2100F field emission transmission electron microscopy operated at 200 kV. UV–vis diffuse reflectance spectrum was recorded with a Shimadzu UV-2500 Spectrophotometer and converted to absorption spectra by the standard Kubelka–Munk method. The surface area measurements were carried out in a Surface Area Analyzer (BELSORP II). The valence state of Cr was analyzed on an X-ray photoelectron spectroscopy (PHI Quantera SXM). Light intensity in the photocatalytic reaction was monitored using a spectroradiometer (USR-40; Ushio Inc., Japan).

2.3. Photocatalytic reaction

In the photocatalytic measurement, a 300 W Xe arc lamp (7 A imported current, focused through a 45 mm × 45 mm shutter window) equipped with a set of glass filters (L42 + HA30, 420 nm < λ < 800 nm, HOYA Co., Japan) and a water filter was used as the light source. Under such condition, the illumination intensity was 30 mW cm^{-2} (ESI, Fig. S12). The 0.2 g of sample was evenly spread over a dish with an area of 8.5 cm^2 in a 500 mL of a borosilicate glass vessel. Then the inside atmosphere of the vessel was exchanged by artificial air [V(N_2):V(O_2) = 4:1] for 10 min to remove gaseous impurities. After the sample was sealed in the vessel, gaseous isopropyl of isopropyl alcohol (IPA) was injected into the vessel (the initial concentration of IPA was about 1250–1500 ppm). Before irradiation, the sample was kept in the dark to ensure an adsorption–desorption equilibrium of IPA on the sample. The final products of the photocatalytic oxidation of IPA were CO_2 and H_2O. To evaluate the photocatalytic activity, the IPA and CO_2 were measured by using a gas chromatography (GC-2014, Shimadzu Corp., Japan) equipped with a methanizer and a flame ionization detector (FID).

3. Results and discussion

3.1. Characterizations of Ag_3PO_4/Cr-$SrTiO_3$ heterojunctions

Fig. 1 shows the X-ray diffraction (XRD) pattern of the as-prepared Ag_3PO_4/Cr-$SrTiO_3$ composite calcined at 500 °C. The

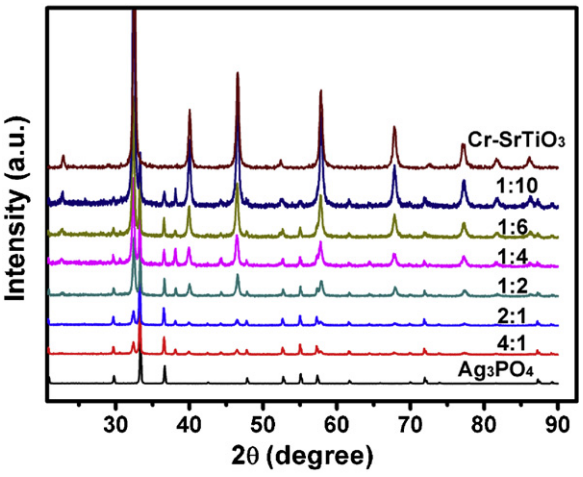

Fig. 1. A comparison of XRD patterns of Cr-$SrTiO_3$, Ag_3PO_4, and Ag_3PO_4/Cr-$SrTiO_3$ composite powders (mass ratio, Ag_3PO_4/Cr-$SrTiO_3$).

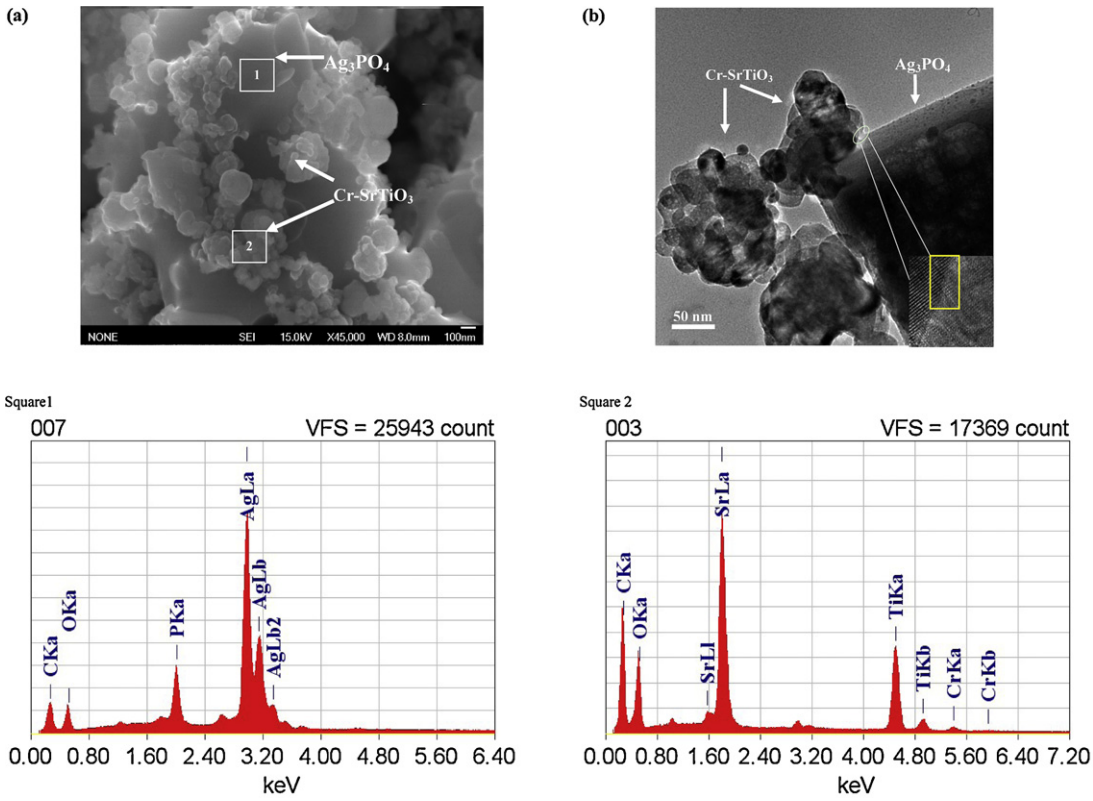

Fig. 2. (a) Typical SEM image and energy dispersive spectra (EDS) pattern of Ag_3PO_4/Cr-$SrTiO_3$ (1:4) composite. The result showed that the composite was composed of Ag_3PO_4 (square 1) and Cr-$SrTiO_3$ (square 2).

indexed diffraction peaks can be ascribed as Ag_3PO_4 and Cr-$SrTiO_3$, respectively. Peaks related to other titanates were not observed in the synthesized samples, indicating that the Ag_3PO_4 did not react with the Cr-$SrTiO_3$. With the increasing the content of the Cr-$SrTiO_3$, the intensities of the Cr-$SrTiO_3$ peaks were increased. Morphologies of the prepared samples were characterized using SEM and TEM. The Ag_3PO_4 phase is composed of particles with sizes from several hundred nanometers to 1 micrometer (see Fig. S2). In contrast, the Cr-$SrTiO_3$ consists of spherical aggregates (~200 nm in diameter) of nanoparticles 30–40 nm in diameter (see Fig. S6). Next, the morphology of the composite (Ag_3PO_4:Cr-$SrTiO_3$ = 1:4) was investigated by SEM–EDX, as shown in Fig. 2(a). For this sample, sub-micropowder particles are partially covered with aggregated nano-particles. Further EDX analysis indicates that former powder and latter particle are Ag_3PO_4 and Cr-$SrTiO_3$, respectively (see Fig. 2(a) square (1) and (2)), which reveals that the Cr-$SrTiO_3$ partially covers on the Ag_3PO_4 surface. To further understand the contact between Ag_3PO_4 and Cr-$SrTiO_3$, TEM observation was applied, as shown in Fig. 2(b). The TEM image indicates that the Ag_3PO_4 and Cr-$SrTiO_3$ are well connected, which is advantageous for the inter-particle photocarrier transfer between Ag_3PO_4 and Cr-$SrTiO_3$. Furthermore, as expected from the particle sizes, the BET surface area of Cr-$SrTiO_3$ is larger than that of Ag_3PO_4 (see Table 1). With an increase in the ratio of Cr-$SrTiO_3$, the BET surface area of the composites also increases.

Fig. 3 shows the UV–vis absorption spectra of Ag_3PO_4, Cr-$SrTiO_3$, and Ag_3PO_4/Cr-$SrTiO_3$ composite. The absorption spectrum of Ag_3PO_4 indicates that it can absorb solar energy with a wavelength shorter than ~530 nm. Moreover, the two absorption edges reveal an indirect band gap of 2.36 eV and a direct transition of 2.45 eV, which are generally in agreement with our previous work [25]. Meanwhile, after doping with Cr (see Fig. S7–8), the absorption edge of Cr-$SrTiO_3$ is a little red-shifted in comparison with that of $SrTiO_3$, which is accordance with the results of previous report [35] (more details see Fig. S9a). In comparison, the visible-light

Table 1
Surface area and pore volume of heterojunctions with different mass ratio.

Mass ratio: (Ag_3PO_4/Cr-$SrTiO_3$)	Surface area ($m^2\ g^{-1}$)	Pore volume ($cm^3\ g^{-1}$)
1:0	0.62	0.14
4:1	2.52	0.57
2:1	4.51	1.03
1:2	10.64	2.44
1:4	11.51	2.64
1:6	14.03	3.22
1:10	15.33	3.35
0:1	16.29	3.71

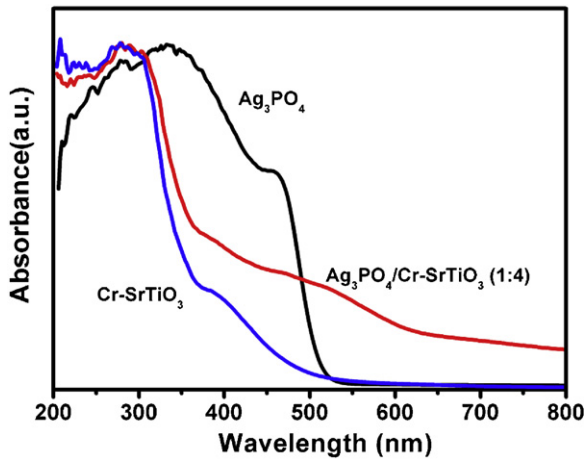

Fig. 3. UV–vis diffuse reflectance spectrum of Cr-$SrTiO_3$, Ag_3PO_4, and Ag_3PO_4/Cr-$SrTiO_3$ (1:4) composite.

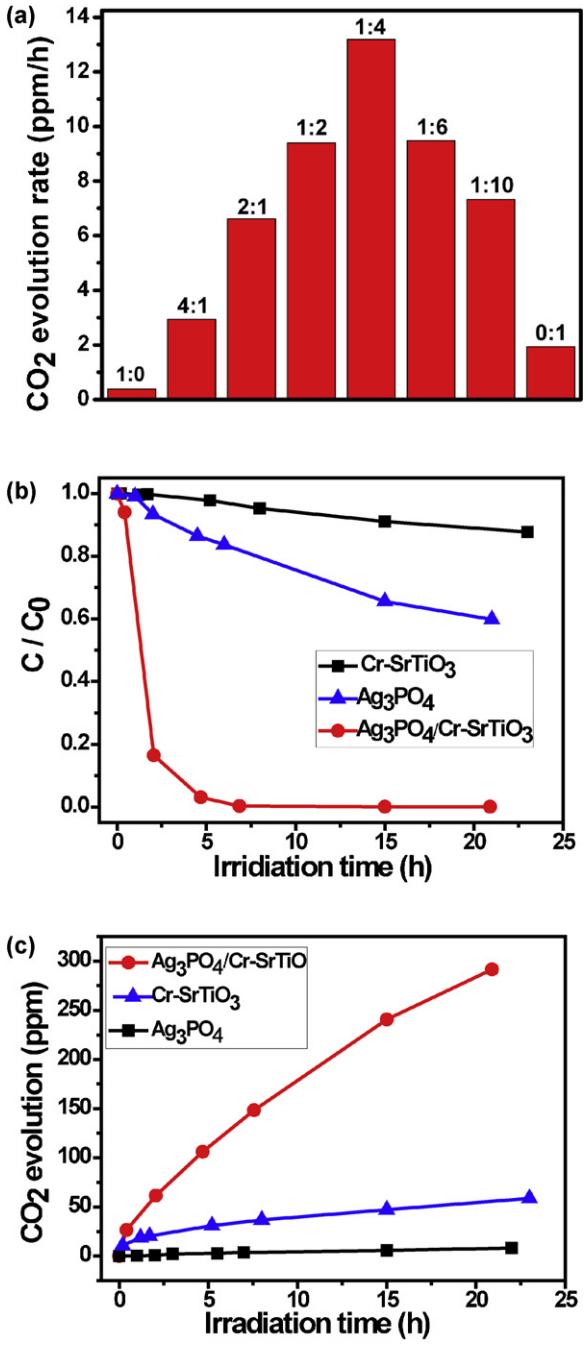

Fig. 4. (a) The photocatalytic conversion activities of of Cr-$SrTiO_3$, Ag_3PO_4, and Ag_3PO_4/Cr-$SrTiO_3$ composite powders (mass ratio, Ag_3PO_4/Cr-$SrTiO_3$), (b) the concentration change of IPA and (c) the evolution of CO_2 over Cr-$SrTiO_3$, Ag_3PO_4, and Ag_3PO_4/Cr-$SrTiO_3$ (1:4) composite powders under visible light irradiation (420 nm < λ < 800 nm).

absorption of Cr-$SrTiO_3$ is obviously weaker than that of Ag_3PO_4. Therefore, the light absorption of the heterojunction is between that of Ag_3PO_4 and Cr-$SrTiO_3$ under 500 nm. On the other hand, the heterojunction exhibits stronger absorption over 500 nm than that of Ag_3PO_4 and Cr-$SrTiO_3$. This absorption could be attributed to the metallic Ag nanoparticles [37,38], which is obtained after the calcination process (see Fig. S9b). For further confirmation, Ag-deposited Cr-$SrTiO_3$ and Ag-deposited Ag_3PO_4 were prepared and characterized (more details see Fig. S10). With changing mass ratios, the absorptions of the heterojunctions were changed but not quite different, and all of the heterojunctions can absorb the light

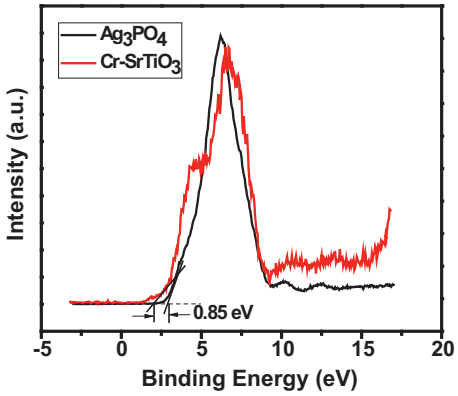

Fig. 5. The VB-XPS spectra of the Cr-$SrTiO_3$ and Ag_3PO_4.

up to 800 nm (see Fig. S11). Therefore, in IPA photodegradation, the Xe lamp was equipped with a UV cut-off to restrict incident radiation to 420–800 nm in the visible light region (see Fig. S12), and with a heat-absorbing filter to avoid the heat effects.

3.2. *Visible light photocatalytic activities and band structure of Ag_3PO_4, Cr-$SrTiO_3$ and Ag_3PO_4/Cr-$SrTiO_3$ heterojunctions*

The photocatalytic conversions of IPA to CO_2 over different photocatalysts were carried out under visible light irradiation (420 nm < λ < 800 nm). As shown in Fig. 4(a), all of the heterostructured samples exhibit different efficiencies with changing the mass ratios. The best activity is obtained at the mass ratio 1:4. To investigate the activity in more details, the degradation of IPA over time for Ag_3PO_4/Cr-$SrTiO_3$ (mass ratio, 1:4) and pure photocatalysts were analyzed (Fig. 4(b)). In the presence of Ag_3PO_4/Cr-$SrTiO_3$ (mass ratio, 1:4) sample, 97% of the IPA is degraded within 3.8 h of irradiation. In contrast, the IPA decomposition ratios are only 9% and 12% over pure Ag_3PO_4 and Cr-$SrTiO_3$ after 8 h of irradiation respectively. Moreover, as shown in Fig. 4(c), the rate of CO_2 evolution over Ag_3PO_4/Cr-$SrTiO_3$ (mass ratio, 1:4) is much higher than that of pure Cr-$SrTiO_3$ and Ag_3PO_4 respectively. There is 291.2 ppm of CO_2 obtained by Ag_3PO_4/Cr-$SrTiO_3$ (mass ratio, 1:4) in comparison with 8.2 ppm and 58.3 ppm achieved by Ag_3PO_4 and Cr-$SrTiO_3$, respectively. Furthermore, recycling reactions for decomposition of IPA over heterojunction samples were carried out under the same conditions. As shown in Fig. S13, decomposition rate of IPA and evolution rates of acetone or CO_2 did not change obviously during the three recycling reactions which indicate that the heterojunction is quite stable during the recycling reactions.

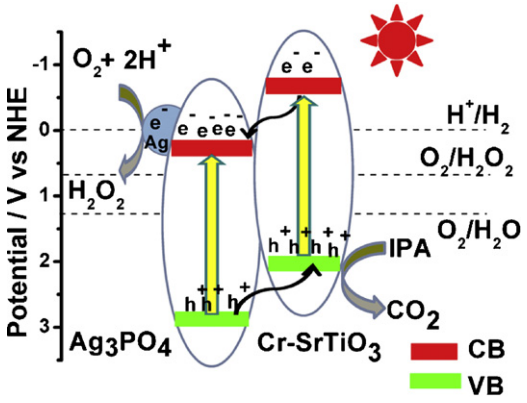

Fig. 6. The Schematic band structure of Ag_3PO_4/Cr-$SrTiO_3$ heterojunction.

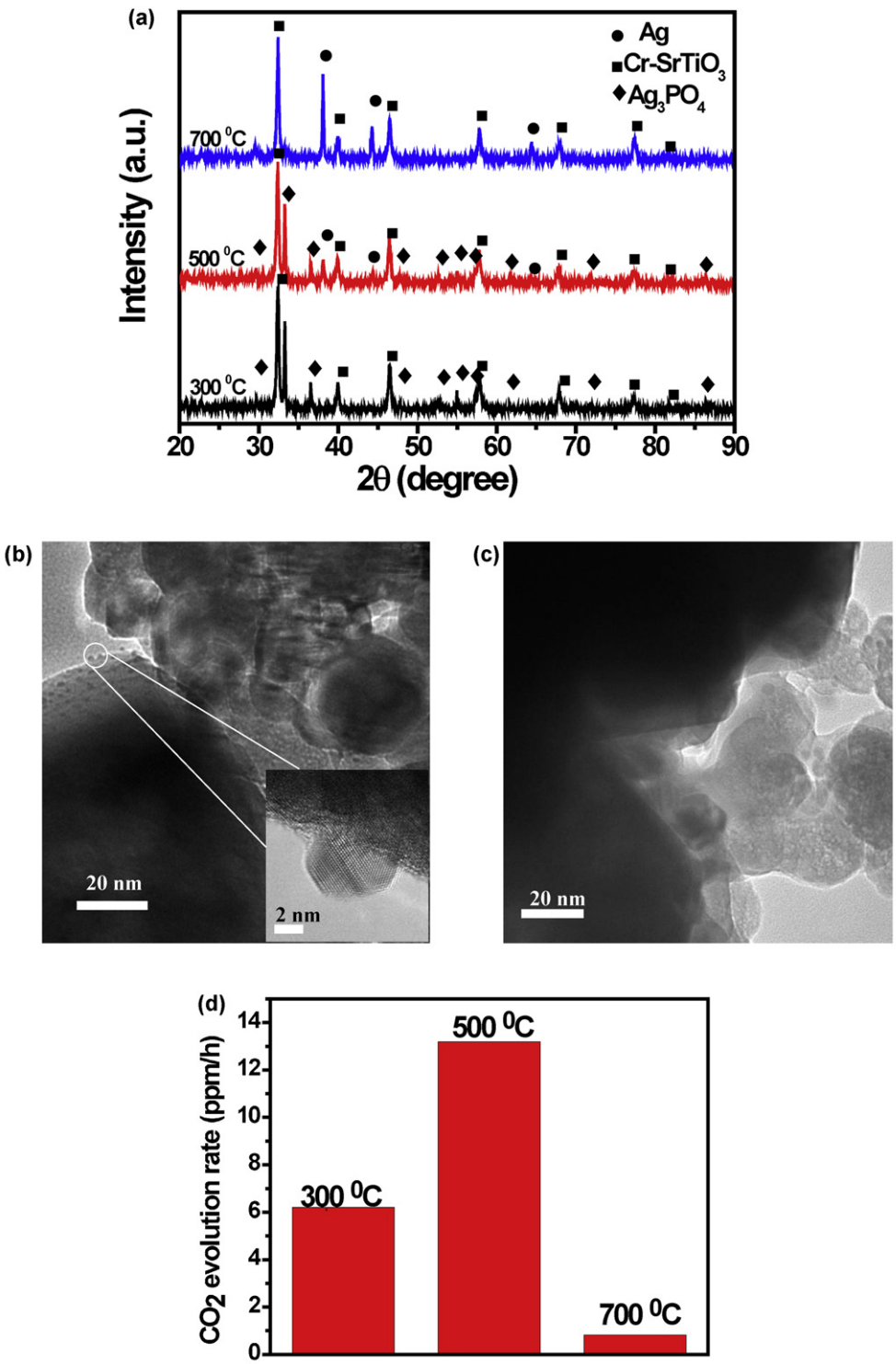

Fig. 7. (a) The XRD patterns and (d) the evolution rate of CO_2 under visible light irradiation of the Ag_3PO_4/Cr-$SrTiO_3$ (1:4) composite powders calcined at different temperature over (420 nm < λ < 800 nm) (i) 300 °C, (ii) 500 °C, and (iii) 700 °C; TEM images of the Ag_3PO_4/Cr-$SrTiO_3$ heterojunction calcined at 300 °C (b) and that of sample calcined at 500 °C (c), inset is the HRTEM image of metallic silver particle and at different temperature.

Since photocatalytic activity is largely dependent on the band structure, the investigations of conduction band (CB) and the valence band (VB) are necessary for understanding the enhanced photocatalytic activity [39,40]. For heterostructured photocatalysts, a good matching of their CB and VB levels can realize the vectorial transfer of photogenerated charge carriers from one to the other, which can contribute to improving the photocatalytic efficiency [41]. The relative positions of the VB tops of Ag_3PO_4 and Cr-$SrTiO_3$ were investigated by comparing their VB X-ray photoelectron spectroscopy (XPS) spectra. As shown in Fig. 5 the VB top of Ag_3PO_4 is 0.85 eV higher than that of Cr-$SrTiO_3$. From our former report [25,26], the band gap of Ag_3PO_4 is 2.45 eV, and its CB and VB positions are +0.45 eV and +2.90 eV (vs. NHE), respectively. Considering the band gap of Cr-$SrTiO_3$ is about 2.5 eV

(see Fig. S9b), the potentials of VB and CB are thus +2.05 eV and −0.45 eV, respectively (see Fig. S9c). The schematic band structure of Ag_3PO_4/Cr-$SrTiO_3$ heterojunction is plotted in Fig. 6. The potential difference between corresponding band levels can drive the charge carriers from one material to its neighbor to form a spatial separation between electrons and holes. In order to confirm the electron transfer between Ag_3PO_4 and Cr-$SrTiO_3$ was really occurred, photocatalytic water splitting over Ag_3PO_4 (0.1 g), Cr-$SrTiO_3$ (0.4 g) and Ag_3PO_4/Cr-$SrTiO_3$ heterojunction (0.5 g, mass ratio, 1:4) were carried out (see Fig. S14). The evolution rate of O_2 over 0.1 g Ag_3PO_4 is about 103.8 μmol h^{-1} and the evolution rate of H_2 over Cr-$SrTiO_3$ is 42.2 μmol h^{-1}. In contrast, the evolution rate of O_2 over Ag_3PO_4/Cr-$SrTiO_3$ heterojunction is only 4.7 μmol h^{-1} and no H_2 been detected over Ag_3PO_4/Cr-$SrTiO_3$ heterojunction. The decreased evolution of O_2 provides a strong evidence to prove that heterostructure has been synthesized between Ag_3PO_4 and Cr-$SrTiO_3$ and generated holes can transfer from Ag_3PO_4 to Cr-$SrTiO_3$ efficiently. Although constructing the heterojunction reduces the redox potentials, the aggregation of electrons and holes over different parts of the heterojunction orients the photochemical reaction to an alternative way which is very advantageous for deeply photodecomposition of IPA to CO_2. The IPA photooxidization undergoes two kinds of typical reaction processes as belows [42,43]:

(i) One-photon reaction

$$CH_3CHOHCH_3 + e^- + O_2 + H^+ \rightarrow CH_3COCH_3 + HO^\bullet + H_2O$$

or

$$CH_3CHOHCH_3 + h^+ \rightarrow CH_3COCH_3 + 2H^+ + e^-$$

(ii) Multiphoton reaction

$$CH_3CHOHCH_3 + 5H_2O + 18\,h^+ \rightarrow 3CO_2 + 18H^+$$

Since the generation of each acetone molecule from IPA usually requires one hole, while the reaction of acetone to CO_2 is a more complex multiphoton-involved process, it is understandable that the photocatalytic decomposition of IPA to acetone is easier than the mineralization of acetone to CO_2 [44]. As shown in Fig. S15, the amount of acetone over pure Ag_3PO_4 is much higher than that of CO_2, which indicates that one-photon reaction take predominance role over Ag_3PO_4. In contrast, due to the aggregated holes of the Ag_3PO_4/Cr-$SrTiO_3$ heterojunction, multiphoton reaction is more easily realized which is signifies the advantage for conversion of IPA to CO_2 (see Fig. 4(c)). Meanwhile, the aggregated electrons of the Ag_3PO_4/Cr-$SrTiO_3$ heterojunction are also beneficial for the reduction of oxygen which plays an important role in the photocatalytic degradation of IPA to CO_2.

3.3. Effects of the calcination temperature and mass ratio on the photocatalytic activity

The effect of the calcination temperature on the photocatalytic activity was also investigated. Fig. 7(a) shows the XRD patterns of the Ag_3PO_4/Cr-$SrTiO_3$ (mass ratio, 1:4) composite powders calcined at 300 °C, 500 °C, and 700 °C. For the sample calcined at 300 °C, there are only Ag_3PO_4 and Cr-$SrTiO_3$ confirmed. With increasing of temperature, the Ag_3PO_4 begins to decompose to produce metallic Ag and completely decomposes by 700 °C. By comparing the TEM images of the samples synthesized at 300 °C and 500 °C (see Fig. 7(b) and (c)), we can find silver particles apparently dispersed on the surface of Ag_3PO_4 (heating at 500 °C). With higher magnification, the inset of Fig. 7(c) shows that the size of nano-silver particle is about 5 nm. As previous research indicated, Ag/silver halide structures, including Ag/AgCl [45], Ag/AgBr [46], and Ag/AgI [47,48], exhibited higher efficiency in organic dye decomposition due to the Ag^0 species that formed during synthesis and irradiation processes could trap the generated electrons. In this work, the metallic silver particles separated out from the surface of Ag_3PO_4 also serve as photogenerated electrons trappers, which is advantageous for the electron transfers and aggregation (as plotted in Fig. 6). Therefore, the multiphoton reaction of IPA photodegradation can be realized more easily. As exhibited in Fig. 7(d), the samples calcined at 500 °C exhibits the best photocatalytic activity. For the sample calcined at 300 °C, there was little metallic silver produced and the contact between the Ag_3PO_4 and the Cr-$SrTiO_3$ particles may be weaker, which make the electron transfer between the two semiconductors difficult. With increasing calcination temperature to 700 °C, the photocatalytic efficiency decreased obviously because of the Ag_3PO_4 completely decomposed. The experiment results reveal that an optimum calcination temperature is an important factor in the preparation of the composite powders with high photocatalytic activity.

The effect of the mass ratio on the photocatalytic activity was also investigated. As exhibited in Fig. 4(a), the photocatalytic activities of the heterostructured samples are closely dependent on the mass ratio of Ag_3PO_4/Cr-$SrTiO_3$. When mass ratio > 1:4, the photocatalytic activity increases; however, when the mass ratio < 1:4, the photocatalytic efficiency decreases. This variation tendency can be explained by the following reasons. One is that Cr-$SrTiO_3$, which is consists of spherical aggregates (~200 nm in diameter) of nanoparticles 30–40 nm in diameter, has high surface area and pore volume (see Table 1). Therefore, increasing the content of Cr-$SrTiO_3$ in the heterojunctions could provide more reactive sites and stronger gas adsorption ability. However, visible-light absorption of Cr-$SrTiO_3$ is obviously weaker than that of Ag_3PO_4, which results in the more content of Cr-$SrTiO_3$ (as shown in Fig. 3), the less visible-light absorption of the heterojunctions. Another reason is that the metallic Ag nanoparticles on the surfaces of Ag_3PO_4 are beneficial for the aggregation of electrons. Moreover, according to the intensity ratios between Ag and the photocatalysts, the amounts of metallic Ag are different in each sample (as shown in Fig. S16(a), Table. S1). Therefore, the variation tendency of the intensity ratio between Ag and Ag_3PO_4 is correlated to that of the photocatalytic efficiency (see Fig. S16(b)). The highest activity was observed on the sample (mass ratio is 1:4, Ag_3PO_4/Cr-$SrTiO_3$) with the intensity ratio (Ag to Ag_3PO_4) is about 0.61.

4. Conclusions

A new heterojunction based on Ag_3PO_4 and Cr-$SrTiO_3$ was designed to attain the efficient elimination of gaseous IPA under visible light irradiation. The study of energy-band potentials via valence-band XPS demonstrated that the potentials of the conduction band (−0.45 eV vs. NHE) and the valence band (+2.05 eV vs. NHE) of the Cr-$SrTiO_3$ are more negative than that of Ag_3PO_4 (+0.45 eV and +2.90 eV, vs NHE, repectively), which is advantageous for the separation and transfer of electrons/holes pairs between these two photocatalysts. The photocatalytic characterizations indicated that the calcination temperature and mass ratio of the Ag_3PO_4/Cr-$SrTiO_3$ dominate the photocatalytic activity of the heterojunctions. All of these heterojunctions could degrade IPA under visible light-irradiation; in particular, the Ag_3PO_4/Cr-$SrTiO_3$ (mass ratio, 1:4, 500 °C) sample showed the highest catalytic performance (CO_2 evolution rate, 13.2 ppm h^{-1}), which was about 33 times higher than that of pure Ag_3PO_4. The present work is evidences that fabricating heterojunctions with proper hand structure to establish a new chemical reaction process is an effective strategy to enhance photocatalytic efficiency or attain new photocatalytic application. The results and discussions herein supply useful informations for further developing the other heterojuction photocatalysts.

Acknowledgment

This work was partially supported by World Premier International Research Center Initiative on Materials Nanoarchitectonics, MEXT.

Appendix A. Supplementary data

Supplementary data associated with this article can be found, in the online version, at http://dx.doi.org/10.1016/j.apcatb.2012.12.038.

References

[1] X. Chen, S. Shen, L. Guo, S.S. Mao, Chemical Reviews 110 (2010) 6503.
[2] A. Kudo, Y. Miseki, Chemical Society Reviews 38 (2009) 253.
[3] H. Tong, S.X. Ouyang, Y.P. Bi, N. Umezawa, M. Oshikiri, J.H. Ye, Advanced Materials 24 (2012) 229.
[4] J.M. Herrmann, Catalysis Today 34 (2005) 49.
[5] S.X. Ouyang, J.H. Ye, Journal of the American Chemical Society 133 (2011) 7757.
[6] T. Inoue, A. Fujishima, S. Konishi, K. Honda, Nature 277 (1979) 637.
[7] I.K. Konstantinou, T.A. Albanis, Applied Catalysis B 49 (2004) 1.
[8] A.L. Linsebigler, G. Lu, J.T. Yates, Chemical Reviews 95 (1995) 735.
[9] R. Asahi, T. Morikawa, T. Ohwaki, K. Aoki, T. Taga, Science 293 (2001) 269.
[10] M. Anpo, N. Aikawa, Y. Kubokawa, M. Che, C. Louis, E. Giamello, Journal of Physical Chemistry 89 (1985) 5017.
[11] S. Sakthivel, H. Kisch, Angewandte Chemie International Edition 42 (2003) 4908.
[12] H. Yu, H. Irie, K. Hashimoto, Journal of the American Chemical Society 132 (2010) 6898.
[13] W. Zhao, W. Ma, C. Chen, J. Zhao, Z. Shuai, Journal of the American Chemical Society 126 (2004) 4782.
[14] D.F. Wang, T. Kako, J.H. Ye, Journal of the American Chemical Society 130 (2008) 2724.
[15] J. Tang, Z.G. Zou, J.H. Ye, Angewandte Chemie International Edition 43 (2004) 4463.
[16] Z. Zou, J.H. Ye, K. Sayama, H. Arakawa, Nature 414 (2001) 625.
[17] I. Tsuji, H. Kato, H. Kobayashi, A. Kudo, Journal of the American Chemical Society 126 (2004) 13406.
[18] H. Yan, J. Yang, G. Ma, G. Wu, X. Zong, Z. Lei, J. Shi, C. Li, Journal of Catalysis 266 (2009) 165.
[19] K. Maeda, T. Takata, M. Hara, N. Saito, Y. Inoue, H. Kobayashi, K. Domen, Journal of the American Chemical Society 127 (2005) 8286.
[20] K. Maeda, K. Teramura, D. Lu, T. Takata, N. Saito, Y. Inoue, K. Domen, Nature 440 (2006) 295.
[21] G. Hitoki, T. Takata, J.N. Kondo, M. Hara, H. Kobayashi, K. Domen, Chemical Communications 16 (2002) 1698.
[22] J. Hensel, G. Wang, Y. Li, J. Zhang, Nano Letters 10 (2010) 478.
[23] X. Zong, H. Yan, G. Wu, G. Ma, F. Wen, L. Wang, C. Li, Journal of the American Chemical Society 130 (2008) 7176.
[24] G. Wang, X. Yang, F. Qian, J. Zhang, Y. Li, Nano Letters 10 (2010) 1088.
[25] (a) Z.G. Yi, J.H. Ye, K. Naoki, K. Tetsuya, et al., Nature Materials 9 (2010) 5352;
(b) Y.P. Bi, J.H. Ye, et al., Chemical Communications 48 (2012) 3748;
(c) Y.P. Bi, et al., Physical Chemistry Chemical Physics 13 (2011) 10071;
(d) Y.P. Bi, et al., Journal of Materials Chemistry 22 (2012) 14847;
(e) Y.P. Bi, et al., Journal of the American Chemical Society 133 (2011) 6490.
[26] N. Umezawa, S.X. Ouyang, J.H. Ye, Physical Review B 83 (2011).
[27] A.J. Bard, R. Parsons, J. Jordan, Standard Potentials in Aqueous Solution, CRC press, 2 Park Square,Milton ParkAbingdon,Oxon,OX14 4RN,UK, 1985.
[28] R.S. Bahadur, S.S. Do, L.W. In, Catalysis Communications 17 (2012) 131.
[29] S. Chu, X.M. Zheng, F. Kong, et al., Materials Chemistry and Physics 129 (2011) 1184.
[30] Y. Wang, T. Yu, X.Y. Chen, et al., Journal of Physics D: Applied Physics 40 (2007) 3925.
[31] H.T. Zhang, S.X. Ouyang, Z.S. Lia, L.F. Liu, T. Yu, J.H. Ye, Z.G. Zou, Journal of Physics and Chemistry of Solids 67 (2006) 2501.
[32] K. Ozawa, Y. Nakao, Z.X. Cheng, D. Wang, et al., Materials Letters 63 (2009) 366.
[33] .S. Girish Kumar, L. Gomathi Devi, Journal of Physical Chemistry A 115 (2011) 13211.
[34] W.F. Yao, B. Zhang, C.P. Huang, et al., Journal of Materials Chemistry 22 (2012) 4050.
[35] D. Wang, J.H. Ye, K. Tetsuya, K. Takashi, Journal of Physical Chemistry B 110 (2006) 15824.
[36] (a) H. Yu, S.X. Ouyang, S.C. Yan, et al., Journal of Materials Chemistry 21 (2011) 11347;
(b) S.X. Ouyang, H. Tong, N. Umezawa, J.Y. Cao, P. Li, Y.P. Bi, Y.J. Zhang, J.H. Ye, Journal of the American Chemical Society 134 (2012) 1974.
[37] J.M. Hermann, H. Tahiri, et al., Applied Catalysis B: Environmental 13 (1997) 219.
[38] G. Lassaletta, A.R. Gonzalez-El, A. Justo, A. Fernandez, F.J. Ager, M.A. Respaldiza, J.C. Soares, M.F. de Silva, Journal of Materials Science 130 (1996) 2325.
[39] B. Xu, W.F. Zhang, X.Y. Liu, J.H. Ye, et al., Physical Review B 76 (2007) 12509.
[40] J. Lv, K. Tetsuya, Z. Zou, J.H. Ye, Applied Physics Letters 95 (2009) 032107.
[41] H.J. Zhang, G.H. Chen, D.W. Bahnemann, Journal of Materials Chemistry 19 (2009) 5089.
[42] Y. Ohko, K. Hashimoto, A. Fujishima, Journal of Physical Chemistry A 101 (1997) 8057.
[43] F. Arsac, D. Bianchi, J.M. Chovelon, C. Ferronato, J.M. Herrmann, Journal of Physical Chemistry A 110 (2006) 4202.
[44] H.F. Shi, X.K. Li, et al., Journal of Physics and Chemistry of Solids 70 (2009) 931.
[45] P. Wang, B. Huang, X. Qin, X. Zhang, Y. Dai, J. Wei, Angewandte Chemie International Edition 120 (2008) 8049.
[46] X. Chen, H.Y. Zhu, J.C. Zhao, Z.F. Zheng, X.P. Gao, Angewandte Chemie International Edition 47 (2008) 5353.
[47] L. Kuai, B. Geng, X. Chen, Y. Zhao, Y. Luo, Langmuir 26 (2010) 18723.
[48] C. Hu, T. Peng, X. Hu, Y. Nie, X. Zhou, J. Qu, H. He, Journal of the American Chemical Society 132 (2010) 857.